ELSEVIER

Journal of Power Sources 109 (2002) 294–300

JOURNAL OF POWER SOURCES

www.elsevier.com/locate/jpowsour

Analysis for electrolytic oxidation and reduction of $PbSO_4$/Pb electrode by electrochemical QCM technique

Masami Taguchi*, Hiroshi Sugita

Department of Materials Science and Engineering, Faculty of Engineering and Resource Science, Akita University, Tegata Gakuennmachi 1-1, Akita 010-8502, Japan

Received 13 August 2001; received in revised form 10 December 2001; accepted 23 January 2002

Abstract

In situ observations of the mass change were carried out using the electrochemical quartz crystal microbalance (EQCM) technique for the active materials in a lead–acid battery during charge–discharge. Lead sulfate was formed on the surfaces of the pure Pb and Pb–Ca–Sn alloys immersed in 4.50 kmol m^{-3} H_2SO_4 solution at 298 K. The rates of $PbSO_4$ formation on the Pb–0.08 mass% Ca–Sn alloys, which are the choice materials for grids in the valve-regulated lead–acid battery (VRLA), were inhibited by the presence of Sn. This fact observed by the EQCM technique was in good agreement with the results determined by the prolonged corrosion test of 604.8 ks at 348 K. This state, in which the $PbSO_4$ exists in the surface and the underlying Pb is not thoroughly reacted, corresponds to the state of active materials after discharge. During electrolytic oxidation, i.e. the charging of the positive electrode, the reaction of $PbSO_4 \rightarrow PbO_2$ could take place to decrease the electrode mass when the current density exceeded a critical value. On the other hand, the reaction of $PbSO_4 \rightarrow Pb$ could readily proceed at just one-fourth the current density of the electrolytic oxidation during the electrolytic reduction of the $PbSO_4$/Pb electrode, i.e. the charging of the negative electrode.

Keywords: Lead–acid battery; Electrochemical QCM technique; Active materials; Charge; Mass change

1. Introduction

It is often said that solar houses will be the mainstream and it will be common sense to install a solar system on the roof in the 21st century. Also, the lead–acid battery is the most suitable secondary battery for storing the electric power generated by the solar system, since the battery is the only one that has demonstrated a satisfactory service life of 10 years or more and its price is significantly lower than those of other batteries [1]. By the way, a float charging, in which the active materials are reactivated by a slight current, is indispensable to prolong the service life of the lead–acid battery. However, most of the investigations on the charge–discharge process of the battery were based on only electrochemical measurements such as voltammetry. There were a few reports that discussed on the basis of in situ observations of the mass change of the specimen, although the mass change measurement is essential for investigation of the surface reactions such as oxidation or reduction. The electrochemical quartz crystal microbalance (EQCM) is an extremely sensitive sensor capable of measuring mass changes in the nanogram range in addition to electrochemical information about potential and current [2,3]. Therefore, this technique is especially suitable for the in situ observations of the charge–discharge reaction of the battery using a small current.

In this report, the kinetics of the $PbSO_4$ formation on pure Pb and Pb–0.08 mass% Ca–Sn alloys, which are the choice materials for the grids of the valve-regulated lead–acid (VRLA) battery [4], were determined in 4.50 kmol m^{-3} H_2SO_4 at 298 K and compared to the results of the prolonged corrosion test at high temperature [5]. The electrolytic oxidation and reduction of the $PbSO_4$/Pb electrode, which was prepared by the immersion of pure Pb in H_2SO_4 solution, was investigated at various current densities using the EQCM technique.

2. Experimental

2.1. Quartz crystal and specimen electrode

An AT-cut quartz crystal with an Au coating on each face was used for the EQCM measurements. The fundamental frequency is 6 MHz. Au, Pb or Pb–Ca–Sn alloy

* Corresponding author. Tel.: +81-18-889-2421; fax: +81-18-889-2421.
E-mail address: taguchi@ipc.akita-u.ac.jp (M. Taguchi).

0378-7753/02/$ – see front matter
PII: S0378-7753(02)00056-3

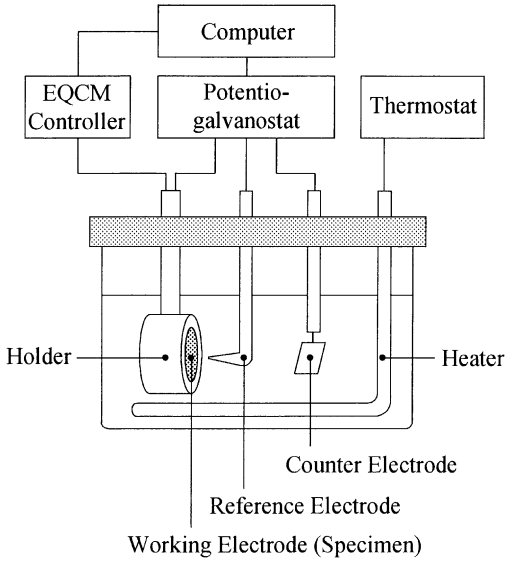

Fig. 1. Experimental apparatus for EQCM measurement.

films were vacuum-evaporated as specimens. It covered the underlying Au completely and directly contacted the solution.

2.2. EQCM measurement

The quartz crystal with the vacuum-evaporated specimen was placed in the holder of the experimental apparatus for the EQCM measurements (Fig. 1). This apparatus consisted of an electrolytic cell, a potentio-galvanostat (Hokuto Denkou, HA-501G), an EQCM controller (Hokuto Denkou, HQ-101B), a thermostat (Yamatake-Honeywell, SA90) and a computer. The counter electrode was a Pt sheet and all potentials were measured versus the Ag/AgCl reference electrode in 3.30 kmol m^{-3} KCl. A (H_2SO_4 + colloidal silica) salt bridge was used in order to avoid the bad influence of chloride ions. Pure Pb and Pb–0.08 mass% Ca–Sn alloy films were vacuum-evaporated as specimens to be immersed in 4.50 kmol m^{-3} H_2SO_4 solution at 298 K for 3.6 ks. The electrolytic oxidation or reduction of the $PbSO_4$/Pb electrode, which was produced by immersing a pure Pb electrode in the H_2SO_4 solution, was then carried out by passing a low current. The potential, current and frequency of the specimen electrode were automatically recorded by a computer with a GP–IB interface during the processes.

2.3. Cyclic voltammetry

Cyclic voltammetry was adopted in order to identify the electrochemical reaction during the electrolytic oxidation and reduction. The potential of the pure Pb electrode was swept three times in the range of −1200 to 2000 mV versus Ag/AgCl to measure the current in the 4.50 kmol m^{-3} H_2SO_4 solution at 298 K.

2.4. X-ray analysis

X-ray photoelectron spectroscopy (JEOL, JPS-9000SX) with Mg Kα radiation was used to analyze the chemical binding of the specimen electrode after immersion or electrolysis. The surface of the specimen was coated with a thin Au film of about 0.3 nm thickness for the calibration of the energy shift, which was caused by the accumulated electrons. The spectrum measurement was repeated after Ar ion etching under the following conditions; the Ar gas pressure, the accelerating voltage and the emission current were 5.0×10^{-2} Pa, 400 V and 6.4 mA, respectively.

3. Results and discussion

3.1. Relationship between frequency change and mass change

Eq. (1) was originally obtained by Sauerbrey [6] to describe that the mass change, dm, is related to the frequency change, df, in a quartz oscillator:

$$\frac{\mathrm{d}m}{\mathrm{d}f} = -\frac{N\rho_\mathrm{q}}{f_0^2} \tag{1}$$

where N is the frequency constant for the AT-cut quartz crystal of 1.67×10^3 Hz m and ρ_q is the density of quartz of 2.65×10^3 kg m^{-3}. Substituting the fundamental frequency, 6 MHz, for the constant f_0 in this equation yields

$$\mathrm{d}m = -1.23 \times 10^{-7}\mathrm{d}f \tag{2}$$

If ρ_Au is the density of a gold, the additional mass of a thin Au film, dm_Au attached to the surface of the quartz crystal by vacuum-evaporation is

$$\mathrm{d}m_\mathrm{Au} = \rho_\mathrm{Au}(t_\mathrm{Au} \times 10^{-9}) \tag{3}$$

where t_Au is the thickness of the thin Au film. Provided that dm = dm_Au and $\rho_\mathrm{Au} = 19.32 \times 10^3$ kg m^{-3}, substitution of Eq. (3) into Eq. (2) yields

$$\mathrm{d}f = -157t_{Au} \tag{4}$$

Fig. 2 shows the relationship between the frequency change of the quartz oscillator and thickness of the vacuum-evaporated Au film. The experimental data in frequency change corresponding to the change in the film thickness is in good agreement with the theoretical value calculated by Eq. (4). Therefore, the authors conclude that Eq. (2) can be used for the conversion of the measured frequency change, df, into the mass change, dm, during the reaction.

3.2. Reactions of pure Pb and Pb–Ca–Sn alloys immersed in sulfuric acid solution

Fig. 3(a) shows the changes in the potential and the mass of a pure Pb film immersed in 4.50 kmol m^{-3} H_2SO_4 solution

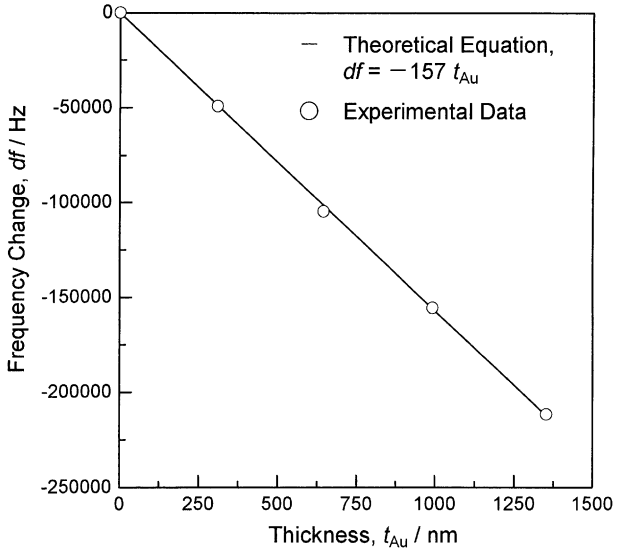

Fig. 2. Relationship between frequency change of quartz oscillator and thickness of vacuum-evaporated Au film in 4.50 kmol m^{-3} H_2SO_4 solution at 298 K.

at 298 K. The potential is stable near −522 mV versus Ag/AgCl right after the immersion, whereas the mass gradually increases with the immersion time. A plot of the mass change as a function of the square root of the immersion time, $t^{1/2}$, reveals a linear relationship over the total immersion time (Fig. 3(b)). Therefore, the reaction of a pure Pb film is concluded to obey the parabolic rate law. A good straight line, passing through the origin in the $dm - t^{1/2}$ plot, was also observed for Pb–0.08 mass% Ca–Sn alloy films. Fig. 4(a) shows the specific reaction rates, K_p (kg m^{-2} $s^{-1/2}$) for the pure Pb, Pb–0.08 mass% Ca, Pb–0.08 mass% Ca–0.20 mass% Sn and Pb–0.08 mass% Ca–1.31 mass% Sn alloy films. The reaction rate of the Pb–0.08 mass% Ca alloy film is greater than that of pure Pb but the rate is reduced with increasing Sn content for the Pb–0.08 mass% Ca–Sn alloys. Moreover, it is noteworthy that a similar tendency is observed between the reaction rate measured by the EQCM technique and the mass gain obtained by the prolonged corrosion test of 604.8 ks in 4.50 kmol m^{-3} H_2SO_4 solution at 348 K (Fig. 4(b)). This similarity suggests

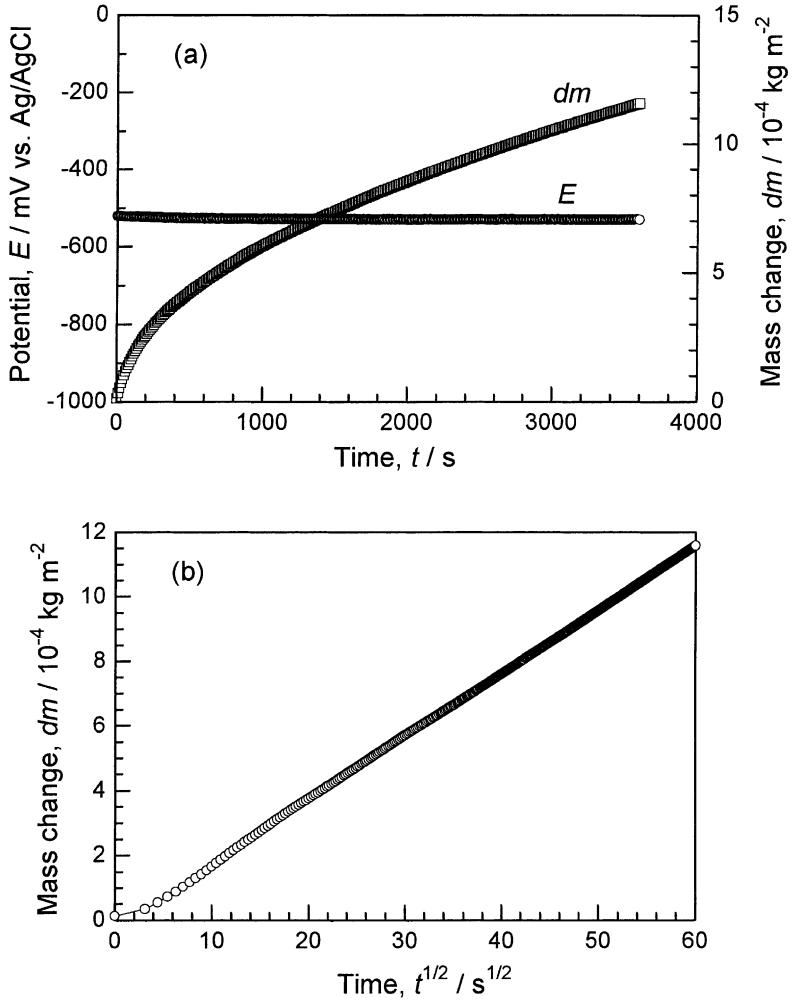

Fig. 3. (a) Changes in potential and mass as a function of immersion time, t and (b) change in mass as a function of square root of immersion time, $t^{1/2}$ for pure Pb film in 4.50 kmol m^{-3} H_2SO_4 solution at 298 K.

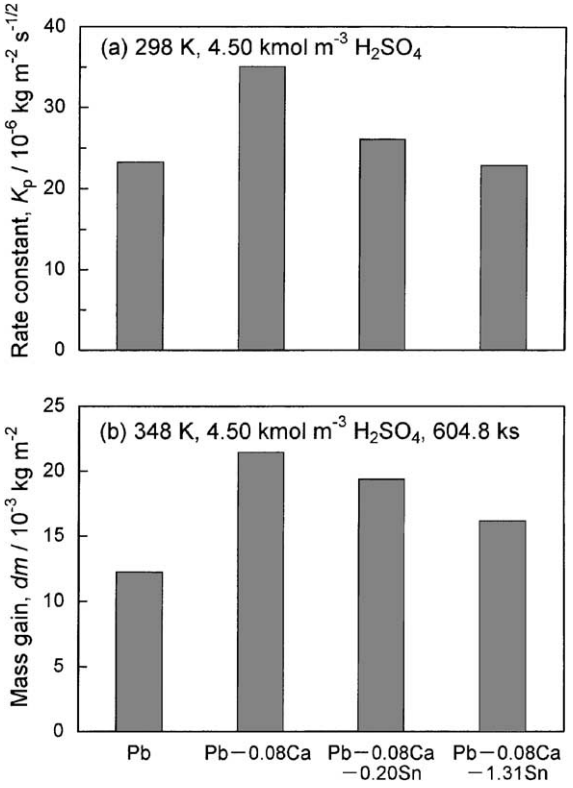

Fig. 4. (a) Specific reaction rates, K_p in 4.50 kmol m^{-3} H_2SO_4 solution at 298 K and (b) mass gains measured by corrosion test of 604.8 ks in 4.50 kmol m^{-3} H_2SO_4 solution at 348 K for pure Pb, Pb–0.08 mass% Ca, Pb–0.08 mass% Ca–0.20 mass% Sn and Pb–0.08 mass% Ca–1.31 mass% Sn alloy films.

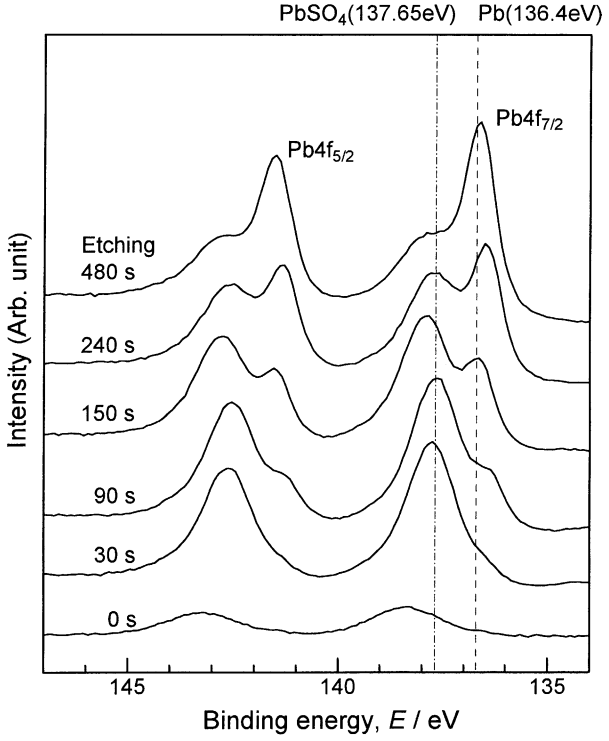

Fig. 5. Pb 4f spectra of pure Pb film immersed for 3.6 ks in 4.50 kmol m^{-3} H_2SO_4 solution at 298 K.

that a short-time measurement by the EQCM technique at room temperature may be used to predict the corrosion behavior of the Pb–Ca–Sn alloys for long-time service at high temperature.

Fig. 5 is the X-ray photoelectron spectra of the pure Pb film electrode immersed for 3.6 ks in 4.50 kmol m^{-3} H_2SO_4 solution at 298 K. The spectra at the etching times of 0 and 30 s have simple peaks and the peaks of the Pb 4f$_{7/2}$ energy level are in agreement with the binding energy of $PbSO_4$, 137.65 eV [7]. At the etching time of 90 s or more, the spectra have shoulder peaks near 136.4 eV. The intensity of the shoulder, whose binding energy agrees with that of metallic Pb [8], rises with the increasing etching time. At the etching time of 240 s or more, the intensity of the metallic Pb surpasses that of $PbSO_4$.

Based on the results of Figs. 3 and 5, a dense $PbSO_4$ layer is formed on the outside of the pure Pb film and the metallic Pb remains unreacted inside. If only the following reaction proceeds, the mass increase, dm, measured by the EQCM technique is a difference in mass between $PbSO_4$ and Pb, or the mass related to SO_4.

$$Pb + SO_4 \rightarrow PbSO_4 + 2e^- \quad (5)$$

Consequently, the reaction ratio of the pure Pb film (thickness: 1122 nm) and the depth of the reacted layer could be calculated to be 19.6% and 220 nm, respectively. The state of the immersed Pb film may correspond to the discharged states of the active materials of the lead–acid battery, i.e. the active material for the positive electrode, PbO_2, is converted into $PbSO_4$ and that for the negative electrode, Pb, turns to be $PbSO_4$ by discharge. Therefore, the pure Pb film was converted to the $PbSO_4$/Pb electrode by immersion and the float charging processes for both the positive and the negative electrodes would be investigated by applying a small current.

3.3. Electrolytic oxidation and reduction of $PbSO_4$/Pb electrode

Fig. 6 shows the changes in both the potential and the mass of the $PbSO_4$/Pb electrode during the electrolytic oxidation and reduction. The electrolytic oxidation was carried out at 7.72×10^{-1} A m^{-2} for the first 1800 s and the reduction was done by switching to -7.72×10^{-1} A m^{-1} in the second 1800 s. During the electrolytic oxidation process, the potential rapidly rises and stabilizes at 1720–1750 mV. During the reduction process, the potential decreases to −555 mV in a short-time but there are two potential plateaus at 1500 and −378 mV during the decrease. On the other hand, the mass of the $PbSO_4$/Pb electrode during the electrolytic oxidation is changed to decrease around 330 s after it had increased. During the reduction process, the mass remarkably increases at an early stage and it is then decreased after 2200 s.

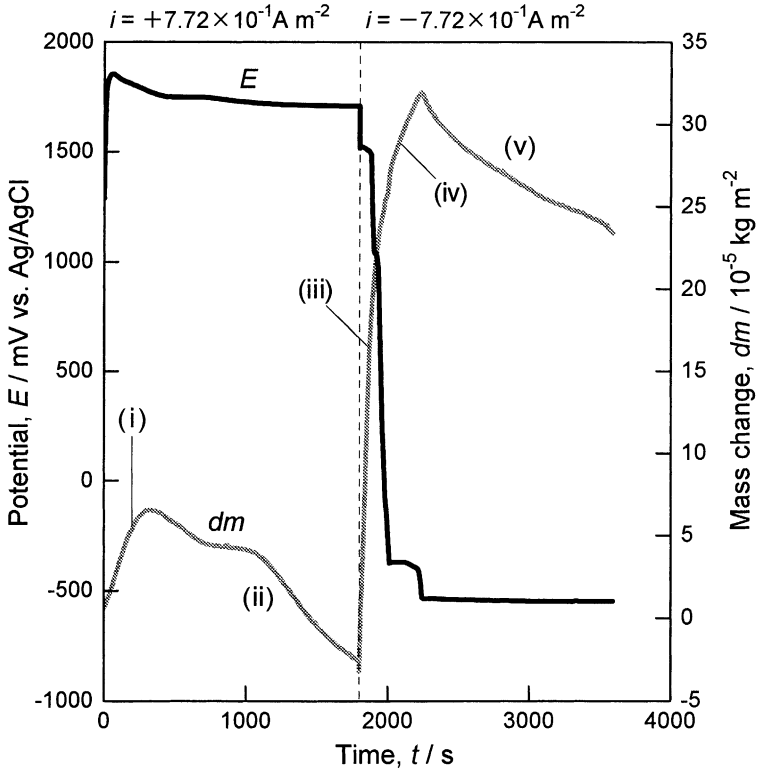

Fig. 6. Changes in potential and mass of $PbSO_4$/Pb electrode during electrolytic oxidation and reduction in 4.50 kmol m^{-3} H_2SO_4 solution at 298 K.

A further examination was required to give a full account of the electrolytic oxidation and reduction phenomena in Fig. 6. Fig. 7 shows the cyclic voltammograms on a pure Pb electrode in 4.50 kmol m^{-3} H_2SO_4 solution at 298 K. When the electrode potential is swept three times in the range of −1200 to 2000 mV versus Ag/AgCl, four anodic current peaks and four cathodic current peaks can be observed. A great deal of fundamental information on the peaks was published in previous papers [4,9–11]. Ruetschi [10] investigated the self-depassivation of lead electrodes after potentiostatic anodization in 4.2 kmol m^{-3} H_2SO_4 solution to reveal at least four characteristic plateaus poten-

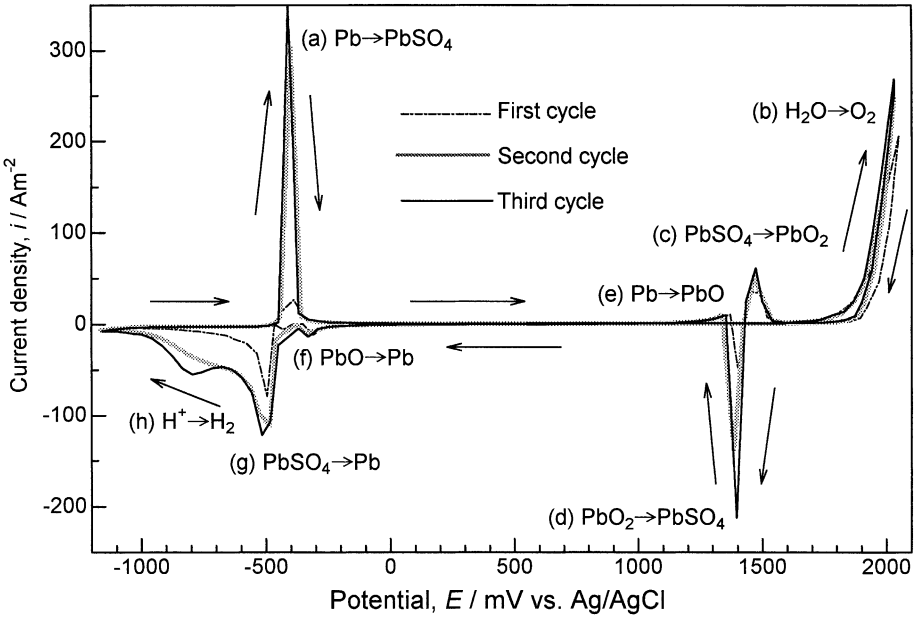

Fig. 7. Cyclic voltammograms on pure Pb electrode in 4.50 kmol m^{-3} H_2SO_4 solution at 298 K.

tials: (1) 1.12 V for $PbO_2/PbSO_4$; (2) ~0.50 V for PbO_2/$PbO{\cdot}PbSO_4$ and/or PbO_2/PbO; (3) −0.38 V for PbO/Pb and/or $PbO{\cdot}PbSO_4$/Pb, and (4) −0.96 V versus Hg/Hg_2SO_4 for $PbSO_4$/Pb potential-determining couple. The plateaus potentials for (1) and (4) coincide with the values observed during the electrolytic reduction of the PbO_2 film electrode produced by a reactive sputtering [12], while the authors can not agree with the potentials for (2) and (3). Pavlov and Iordanov [11] established the growth processes of the anodic crystalline layer on potentiostatic oxidation of lead in a sulfuric acid. When the oxidation potentials exceeded 0.95 V versus Hg/Hg_2SO_4, α-PbO_2 formed in addition to *tert*-PbO. At the potentials more positive than 1.00 V versus Hg/Hg_2SO_4, the solute Pb^{2+} ions oxidized to β-PbO_2 at α-PbO_2/solution interface in 1 N H_2SO_4 solution. Taking into account of the results mentioned, the anodic current peaks can be identified as the oxidation of Pb to $PbSO_4$, peak (a); the evolution of O_2, peak (b); the oxidation of $PbSO_4$ to PbO_2, peak (c) and Pb to PbO, peak (e). On the other hand, the cathodic current peaks are able to be explained as the reduction of PbO_2 to $PbSO_4$, peak (d); PbO to Pb, peak (f); $PbSO_4$ to Pb, peak (g) and the evolution of H_2, peak (h).

The mass change of the $PbSO_4$/Pb electrode in Fig. 6, can be explained on the basis of the cyclic voltammograms. As the reactions (a) Pb → $PbSO_4$ and (b) Pb → PbO occur, the mass of the $PbSO_4$/Pb electrode increases at the beginning of the electrolytic oxidation (Section I). However, the potential soon reaches the level that the reaction (c) $PbSO_4 \rightarrow PbO_2$ occurs. The conversion of the mass from increasing to decreasing is observed near 300 s, when the latter reaction becomes more active than the two former reactions (Section II). On the other hand, only the reaction (d) $PbO_2 \rightarrow PbSO_4$ occurs and the mass of the electrode significantly increases early in the electrolytic reduction from 1800 to 2000 s (Section III). There is a decline in the mass increase from 2000 to 2200 s (Section IV), because the potential remains at −378 mV and the reduction of (f) PbO → Pb occurs. The mass of the electrode then decreases as the electrode potential decreases to −555 mV and the reaction (g) $PbSO_4 \rightarrow Pb$ proceeds (Section V). And, there is a possibility that the oxygen and hydrogen evolution partly occur in Sections II and III, respectively.

3.4. Influence of applied current density on electrolytic oxidation and reduction

Fig. 8 shows the electrode potential and the mass change in the $PbSO_4$/Pb electrode during the electrolytic oxidation at various current densities in the 4.50 kmol m^{-3} H_2SO_4 solution at 298 K. Here, the electrolytic oxidation was done in succession. In short, the current of 4.83×10^{-1} A m^{-2} was applied to the $PbSO_4$/Pb electrode immediately after the electrolytic oxidation of 9.65×10^{-2} A m^{-2}. When the current density is equal to or less than 9.65×10^{-1} A m^{-2}, the potential of the $PbSO_4$/Pb electrode is constant near −530 mV. At this potential, it is possible to estimate that

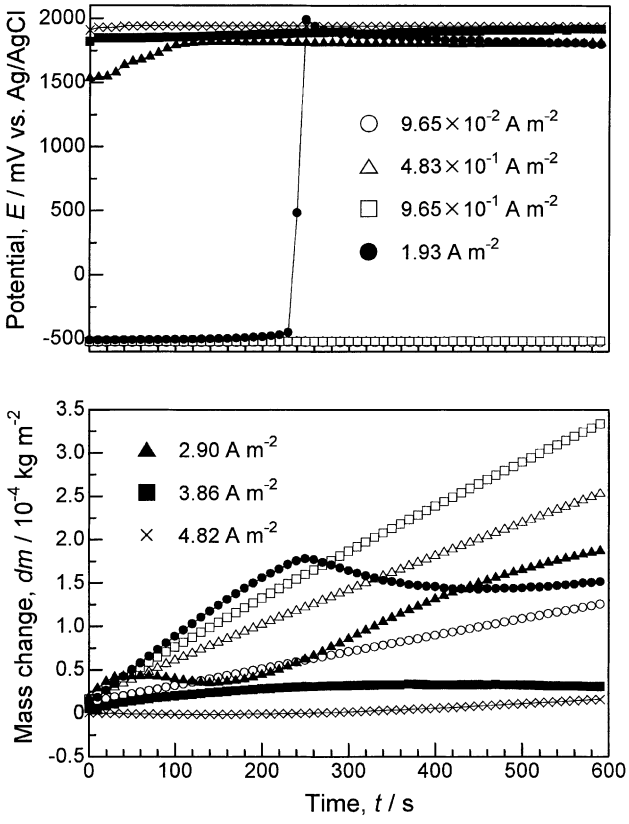

Fig. 8. Changes in potential and mass of $PbSO_4$/Pb electrode during electrolytic oxidation at various current densities in 4.50 kmol m^{-3} H_2SO_4 solution at 298 K.

only the reaction Pb → $PbSO_4$ occurs. In fact, the mass linearly increases and the increasing rate is enhanced with the increasing current density. However, the electrode potential at the current density of 1.93 A m^{-2} suddenly rises to 2000 mV at about 230 s. Corresponding to the change in the electrode potential, the mass of electrode switches from an increase to a decrease. For the current densities of 2.90–4.82 A m^{-2}, the potentials are kept at the high level of 1800–2000 mV and the amount of the mass gain decreases with the increasing current density. At these potentials, the three reactions: Pb → $PbSO_4$, Pb → PbO and $PbSO_4 \rightarrow PbO_2$ are capable of occurring. However, it can be interpreted that the mass significantly decreases at high current densities because of the predominant reaction of $PbSO_4 \rightarrow PbO_2$.

Fig. 9 shows the electrode potential and the mass change of the $PbSO_4$/Pb electrode during electrolytic reduction. The electrolytic reduction was carried out in succession, like the electrolytic oxidation. The potential of the $PbSO_4$/Pb electrode is steady in the range of −530 to −550 mV versus Ag/AgCl, although the applied current density increased from -9.65×10^{-2} to -9.65×10^{-1} A m^{-2}. At these potentials, both the reactions, $PbO_2 \rightarrow PbSO_4$ and PbO → Pb, are capable of proceeding in addition to the reaction $PbSO_4 \rightarrow Pb$. However, we must take into account the fact that the PbO_2 and the PbO phases were scarcely detected in the original elec-

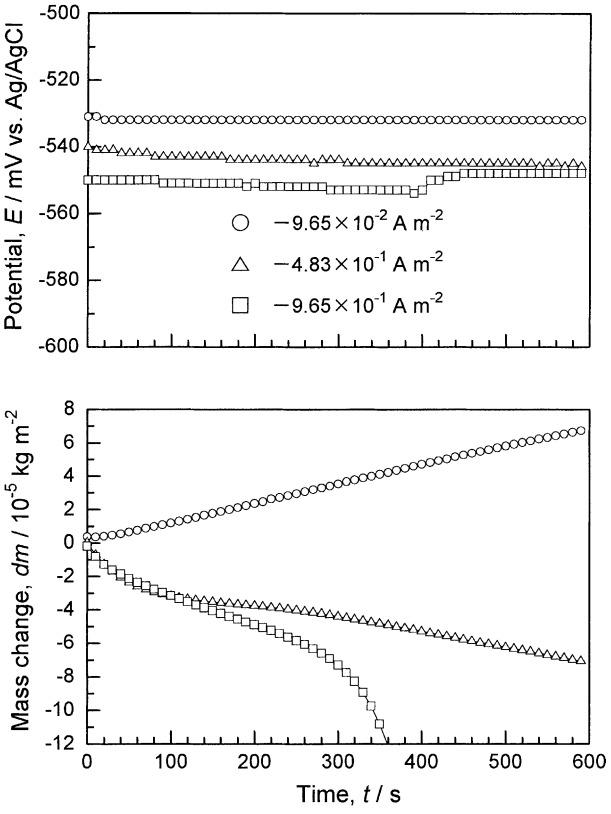

Fig. 9. Changes in potential and mass of $PbSO_4$/Pb electrode during electrolytic reduction at various current densities in 4.50 kmol m^{-3} H_2SO_4 solution at 298 K.

trode. On the other hand, the mass of the $PbSO_4$/Pb electrode increases at the current density of -9.65×10^{-2} A m^{-2} but the slight increase in the current density to -4.85×10^{-1} A m^{-2} brings about a decrease in the electrode mass. Since the original electrode has little PbO_2 and PbO, the mass gain of the $PbSO_4$/Pb electrode at -9.65×10^{-2} A m^{-2} may be caused by the reaction $Pb \rightarrow PbSO_4$ under immersion or the adsorption of ions. At the current density of -4.85×10^{-1} A m^{-2} or more, the reaction $PbSO_4 \rightarrow Pb$ can be found to decrease the mass. It must be noted that the current density is just one-fourth of the critical value that the reaction $PbSO_4 \rightarrow PbO_2$ requires by charging of the positive electrode. Therefore, it may be concluded from the in situ observation using the EQCM technique that the charging reaction of the negative electrode more readily occurs than that of the positive electrode.

4. Conclusion

The kinetics of $PbSO_4$ formation on pure Pb and Pb–0.08 mass% Ca–Sn alloys, and the electrolytic oxidation and reduction of the $PbSO_4$/Pb electrode were investigated by the EQCM technique in a 4.50 kmol m^{-3} H_2SO_4 solution at 298 K. The results are summarized as follows:

1. The formation rate of $PbSO_4$ on the Pb–0.08 mass% Ca–Sn alloys immersed in the sulfuric acid solution is inhibited by the presence of Sn. This fact can be confirmed by the short-term EQCM measurements at room temperature, as well as by a long-term corrosion test at high temperature, i.e. in the 4.50 kmol m^{-3} H_2SO_4 solution at 348 K for 604.8 ks.
2. During the charge of the positive electrode, i.e. the electrolytic oxidation of the $PbSO_4$/Pb electrode, only the reaction $Pb \rightarrow PbSO_4$ proceeds at a low current density. If the applied current density exceeds a critical value, the reaction $PbSO_4 \rightarrow PbO_2$ can take place and decrease the electrode mass. On the other hand, during the charging of the negative electrode, i.e. the electrolytic reduction of the $PbSO_4$/Pb electrode, the reaction $PbSO_4 \rightarrow Pb$ can readily proceed at just one-fourth the current density for charging of the positive electrode.

Acknowledgements

The authors acknowledge the financial support from the Grant-in-Aid for Scientific Research by Japan Society for the Promotion of Science (13875142) for carrying out this study.

References

[1] T. Takamura, Electrochemistry 68 (2000) 615–619.
[2] S. Bruckenstein, M. Shay, Electrochim. Acta 30 (1985) 1295–1300.
[3] F. Gan, Z. Dai, D. Wang, L. Yao, Corros. Sci. 42 (2000) 1379–1388.
[4] T. Hirasawa, K. Sasaki, M. Taguchi, K. Kaneko, J. Power Sources 85 (2000) 44–48.
[5] M. Taguchi, Y. Hiramatsu, T. Hirasawa, N. Tanaka, J. Jpn. Inst. Met. 65 (2001) 727–732.
[6] G. Sauerbrey, Z. Phys. 155 (1955) 206–222.
[7] L. Ley, S.P. Kowalczyk, F.R. McFeely, R.A. Pollak, D.A. Shirley, Phys. Rev. B8 (1973) 2392–2397.
[8] M. Taguchi, T. Hirasawa, J. Jpn. Inst. Met. 61 (1997) 77–82.
[9] V. Danel, V. Plichon, Electrochim. Acta 28 (1983) 781–784.
[10] P. Ruetschi, J. Electrochem. Soc. 120 (1973) 331–336.
[11] D. Pavlov, N. Iordanov, J. Electrochem. Soc. 117 (1970) 1103–1109.
[12] M. Taguchi, Unpublished data.